Neutron scattering investigation of low-momentum collective ion dynamics in liquid potassium

L. E. Bove,[1] B. Dorner,[2] C. Petrillo,[3] F. Sacchetti,[1] and J.-B. Suck[4]
[1]*INFM and Dipartimento di Fisica, Universitá di Perugia, Via Alessandro Pascoli, I-06123 Perugia, Italy*
[2]*Institut Laue Langevin, Boîte Postale 156, F-38042 Grenoble Cedex 09, France*
[3]*INFM and Dipartimento di Fisica, Politecnico di Milano, Piazza Leonardo da Vinci 32, I-20133 Milano, Italy*
[4]*Institute of Physics, Material Research and Liquids, TU Chemnitz, D-09107 Chemnitz, Germany*
(Received 5 February 2003; revised manuscript received 2 April 2003; published 31 July 2003)

The low-momentum collective ion dynamics of molten potassium has been investigated by means of a high-resolution inelastic neutron-scattering experiment. Collective vibrational modes were found to contribute to the coherent response function over the wave-vector transfer region from 0.2 up to 1 $Å^{-1}$. The analysis of the quasielastic features of the dynamic structure factor, due to mainly incoherent scattering, suggests that contributions other than the expected self-diffusion are present. An internally consistent description of the low momentum collective ion dynamics in molten alkali metals was obtained by applying the same data analysis scheme to the present data and those published on Li, Na, Rb, and Cs. The main conclusion is that the Bohm-Staver prescription for the collective-mode velocity does not describe the whole alkali metals series and approaches beyond the random-phase approximation are necessary to treat the electron gas screening of the ion interactions.

DOI: 10.1103/PhysRevB.68.024208 PACS number(s): 61.12.−q, 61.25.Mv, 71.10.Ay, 78.70.Nx

I. INTRODUCTION

The theoretical treatment of the dynamic correlations in liquid simple metals, extending from the hydrodynamic to the microscopic kinetic regimes, can be considered one of the long-standing problems in the physics of dense fluids. A classical criterion for testing the validity of different liquid state theories is their ability to describe the dynamic response function as measured by inelastic neutron, and more recently inelastic x ray, scattering in the simplest among liquid metals, that is, alkali metals. Alongside with some historical experiments such as that of Copley and Rowe on rubidium,[1] which, about 30 years ago, showed unambiguously the existence of collective excitations extending well beyond the hydrodynamic regime, the experimental investigation of these systems has progressed continuously until the very recent measurement of Cabrillo *et al.* on molten potassium.[2] At present, the dynamic properties of all the elements belonging to the alkali-metals group have been investigated by inelastic neutron scattering,[1–7] and in the case of lithium and sodium also by x-ray scattering experiments.[8,9] An overall evidence for the occurrence of collective excitations, namely, propagating ion density fluctuations with an associated dispersion relation extending typically up to half the position of the first maximum of the static structure factor, has been reported for all the alkali metals.

Theoretical modeling of the reported experimental findings has commonly exploited analytic approaches, such as those provided by the kinetic[10] and mode-coupling[11] theories of liquids, or computational schemes made more and more effective by the advances in computer simulation techniques. Formal schemes, however, maintain an appealing character because of the physical insight into the microscopic mechanisms governing the liquid dynamics. This explains the success of the memory-function[12] based approach for calculation of the time correlation functions, although practical applications of this technique typically rely on short-time expansions of the relevant correlation functions.[13,14] The viscoelastic model,[13,14] which can be derived from a continued fraction representation of the memory function, and the more recent semiempirical[8] and ''beyond-viscoelastic''[2] schemes for the memory function have been applied to liquid simple metals. These approaches provide a satisfactory description of the dynamic behavior, although the mechanisms of time decay of the memory functions are not sensitive to the different nature of the interaction potential or to more subtle quantum effects.

Experimental investigation of the dynamic response in alkali metals, carried out at the highest accuracy level enabled by the present top-performance scattering instrumentation, should clarify the microscopic mechanisms behind the ion density fluctuations and their link to the details of the interatomic potential. In particular, the role of the electron density related effects against the short-range ion size dependent interactions can be inspected by studying the ion dynamics of liquid alkali metals, that is, systems, which in the liquid phase can be featured as a two-component plasma of interacting electrons and ions,[15] while in the solid bcc phase are characterized by a simple electronic structure and mostly ''harmonic''- vibrational spectra. Experimental evidence for the electron-gas driven effects on the ion dynamics was obtained[16] by recognizing a scaling relation, based on the scaling of the electron density, in the dispersion curves associated with the collective excitations of liquid Rb,[1] Cs,[7] and a properly tailored K-Cs alloy.[16] The analysis of the dispersion curves and the mode velocities was carried out by means of a simple Bohm-Staver (BS) model for the coupled electron-ion plasma,[15,17] which has the merit of emphasizing the role of the electron-gas density although through a simplified description of the electron-screened ion-ion Coulomb interaction. Rather surprisingly, the BS prediction of the collective-mode velocity was found to properly describe the experimental findings in two polyvalent and high electron-density samples such as liquid lead and mercury,[18] where the

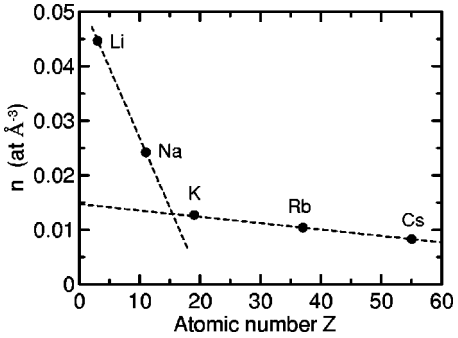

FIG. 1. Atomic number density n of alkali metals at melting point versus the atomic number Z. Dashed lines are guides to the eye.

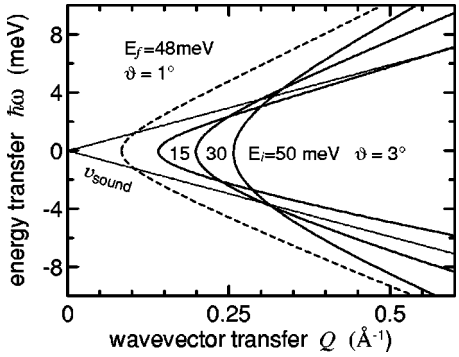

FIG. 2. Low wave-vector transfer portion of the kinematic region $(Q,\hbar\omega)$ accessible to the investigation of Ref. 2 at the three incoming neutron energies 15, 30, and 50 meV of the experiment and the lowest scattering angle of the instrument, i.e., 3° (continuous lines). The low-Q kinematic region of the present experiment, with 48 meV final neutron energy and 1° scattering angle, is also shown (dashed line). The dotted line is the sound dispersion.

ion core repulsive potential was expected to play a major role. However, the most striking effect of the electron correlations on the ion dynamics seems that observed in a saturated metal solution of lithium ammonia,[19,20] a system characterized by a very low electron density (well beyond the limit of the typical metallic region) and, hence, by electron-electron interactions dominating over the kinetic energy.[17,21] Indeed, an anomalous and rather abrupt decrease of the energy of the collective mode was observed at a wave-vector transfer close to $2k_F$, where k_F is the Fermi wave vector. This behavior is compatible with the singularity at $2k_F$ of the electron-gas dielectric function resulting in the Kohn anomaly in a system with an isotropic spherical Fermi surface, and it was interpreted[20] in terms of electron interactions as modeled by a dielectric function beyond RPA (random phase approximation).[21]

The view of alkali metals and their solutions as the closest systems approximating the interacting two-component plasma, despite the perturbing presence of finite-size ion cores, makes the investigation of the low-frequency dynamics of these liquid systems a rare opportunity to obtain experimental information on the electron screening of the ion-ion Coulomb interactions, and possibly on the wave-vector dependent dielectric function $\epsilon(Q)$ of the homogeneous interacting electron gas.

Among alkali metals, potassium occupies a position in the periodic table which suggests for it a key role in drawing a comprehensive view of the properties of all these metals. This is apparent from Fig. 1 where the atomic number density of alkali metals near the melting temperature T_m is plotted versus the atomic number: an abrupt change in the trend occurs close to the potassium position. Indeed, the atomic number density of potassium is low and close to that of the heavier rubidium and cesium, while lithium and sodium, the lighter ones, have a much higher number density. Since the atomic number density is directly related to the repulsive potential, the trend observed in Fig. 1 emphasizes that K, Rb, and Cs are described by a similar repulsive potential which differs from that of Li and Na. This suggestion could be checked by extending to potassium the BS analysis which amounts to neglecting the effect of the ion size on the propagating collective mode and resulted in the mentioned scaling relation for Rb, Cs, and K-Cs.[16] Therefore, a detailed investigation of the low-frequency and low-momentum dynamics of liquid potassium seems to be extremely appropriate. It is also noteworthy that the critical density and the viscosity at the melting point[22] exhibit an anomaly on potassium. Moreover, the static structure factor of liquid potassium has been measured[23] and lattice-dynamics data for the crystal are available.[24] On the theoretical side, the available calculations of both the static structure factor in the liquid[25] and the dynamic structure factor in the solid up to the melting point[26] were based on the use of semiempirical pair potentials. Recently, a path-integral molecular-dynamics method[27] has been applied to study the temperature dependence of both structural and dynamic properties of potassium. An advantage of this approach lies in clarifying the coupling between the atomic and the electronic structure.

Inelastic neutron data on potassium taken close to T_m had been reported previously.[5] However, the restricted wave-vector and energy-transfer range $(Q,\hbar\omega)$ prevented an extended analysis of the ion dynamics and the rather high-Q values, namely, $1 \leqslant Q \leqslant 1.3$ Å^{-1}, were not optimized to observe the presence of collective excitations which are expected to be more visible at low wave vectors. An extended experimental study of the dynamic response in molten potassium has been published quite recently.[2] The authors exploited a combination of different inelastic neutron-scattering techniques to measure the quasielastic and the inelastic contributions to the dynamic response, aiming at separate modeling of the diffusive atomic motions and the collective density oscillations. The low-Q portions of the kinematic region $(Q,\hbar\omega)$ explored in the experiment of Ref. 2, corresponding to the three different incident neutron energies 15, 30, and 50 meV, and calculated at the minimum scattering angle attainable by the instrument used (MARI at the ISIS Spallation Source, U.K.), namely, 3°, are shown in Fig. 2 in comparison with the linear dispersion associated with the isothermal sound velocity.[22] An experiment aiming for the investigation of the collective excitations in liquid potassium would certainly benefit from accessing an even lower-Q region. This is possible by using a three-axis spectrometer[16,18,20] which combines the demand for high-energy resolution with the

possibility of measuring the cross section at scattering angles as low as 1°. The kinematic region corresponding to the three-axis configuration of the present experiment, that is, 48 meV fixed final energy and 1° scattering angle, is also shown in Fig. 2 for comparison.

In the present paper, we report on the high-resolution inelastic neutron scattering investigation of the low-frequency and low-wave-vector dynamics of potassium at 350 K ($T_m = 336$ K). The purpose of the investigation is twofold: first to obtain an accurate determination of the dynamic structure factor in the low-wave-vector region; second to deduce the velocity associated with the density fluctuations by analyzing the linear portion of the dispersion curve of collective modes. Since we believe that the data on potassium are crucial to emphasize the presence of trends common to all the molten alkali metals or to point out at possible discontinuities, thanks to the special position of this element within the series, we analyzed the present data by applying the already tested BS model as a key to identify the dependence of the dynamic properties on the electron gas. In order to draw model-independent conclusions from the experimental data, we extended the present analysis procedure to the published data on molten alkali metals. The comparative analysis of the low-momentum dynamics showed that the BS prescription fails in predicting the absolute value of the mode velocity in molten alkali metals, which discards the possibility of an overall scaling of all the alkali metals based on the long-wavelength RPA representation of the electron dielectric function and shows that the RPA scheme does not provide an adequate representation of the electron-gas screening effects.

II. EXPERIMENT AND DATA ANALYSIS

The inelastic neutron-scattering measurements were carried out at the hot and thermal-neutron three-axis spectrometer IN1 installed at the High Flux Reactor of the Institut Laue Langevin (ILL, Grenoble, France). The spectrometer configuration was optimized to achieve high-energy resolution in conjunction with operation at low scattering angles (1°) and still acceptably high incoming intensity. Tight Soller collimations of 25′, 20′, 20′, and 30′ from the reactor to the detector were chosen for coupling to two wide vertically focusing crystals, namely, a (200) Cu monochromator and a (004) PG analyzer. The instrument was operated at fixed final energy with the analyzer set to select the neutron wave vector $k_f = 4.8$ Å^{-1}. A remarkable reduction of the background in the small-angle configuration was accomplished by means of an evacuated flight path, namely, a 1-m-diameter chamber, around the sample.

The sample was a 99.9% pure potassium ingot (Sigma, Aldrich) with natural isotopic composition, which was manipulated, weighted, and sealed into the cell, under the inert atmosphere of a He-filled glovebox. The cell, specially designed for this experiment, was slab shaped, vacuum tight aluminum container, $70\times40\times20$ mm^3 size and 0.5 mm wall thickness. To reduce the amount of multiple scattering from the sample, which, nonetheless, was expected to be rather small, six horizontal highly absorbing Gd blades of 0.25 mm thickness were mounted inside the cell at equal distance. At

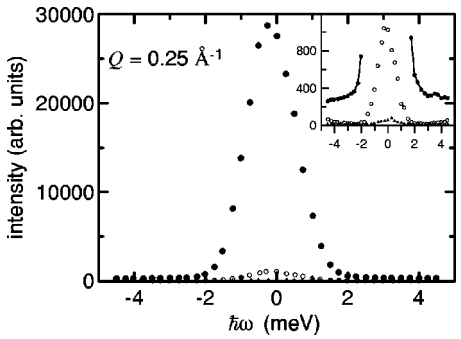

FIG. 3. Raw intensity versus energy transfer as measured at wave-vector transfer $Q = 0.25$ Å^{-1} on molten potassium (dots), the empty alumnum cell (circles), and a full absorbing cadmium plate (triangles). The data are shown also in the inset on an expanded scale to emphasize the very low background contribution.

the temperature of the experiment, that is, 350 K, no alloying between K and Gd and K and Al was expected.[28] The sample temperature was measured with an accuracy of 0.01° by means of two Pt sensors, which were inserted into two small holes on top and bottom of the aluminum cell. Heating of the potassium sample at 350 K, i.e., just above the melting point, was achieved by means of four resistive elements placed at the top and bottom edges of the cell, and coupled to a standard ILL temperature controller. The temperature was stable within 0.1°, although it was not constant along the 70 mm length of the cell; indeed, a maximum temperature gradient of ~3° was registered by the top and bottom Pt sensors.

Inelastic scans from the sample were collected at nine values of wave-vector transfer, namely, $Q = 0.2$, 0.25, 0.35, 0.5, 0.65, 0.75, 0.85, 1.0, and 1.2 Å^{-1}. Background scans were carried out on a second identical, but empty, aluminum cell, at the same Q values as the sample. The environment background was measured by collecting inelastic scans at $Q = 0.2$, 0.25, 0.5 and 0.75 Å^{-1} on a fully absorbing cadmium plate with the same size as the sample and 2 mm thickness. As an example, the intensities measured from the sample, the empty cell and the cadmium plate at $Q = 0.25$ Å^{-1} are shown in Fig. 3. The contribution from the aluminum cell was dominated by the central peak, originating from elastic processes, with tails of negligible intensity. The background contribution arising from the environment was very low as demonstrated by the measurements on the absorbing Cd plate. To measure the elastic resolution of the spectrometer and to normalize the intensity data, an inelastic scan at $Q = 0.5$ Å^{-1} was carried out on a standard vanadium plate having a thickness equal to 1.5 mm and contained inside the Al cell. The vanadium spectrum was very well reproduced by the theoretical resolution function, calculated for the specific configuration of the instrument according to Ref. 29. It resulted in a Gaussian function with a full width at half maximum (FWHM) equal to 1.50 meV. The experimental data are shown in Fig. 4 in comparison with the calculated resolution function. The excellent agreement is apparent. To point out at the effects of the instrument resolution on the sample data, the measured vanadium spectrum and its Gaussian fitting function are shown in Fig. 5 against the raw potassium data at the same wave-vector transfer Q

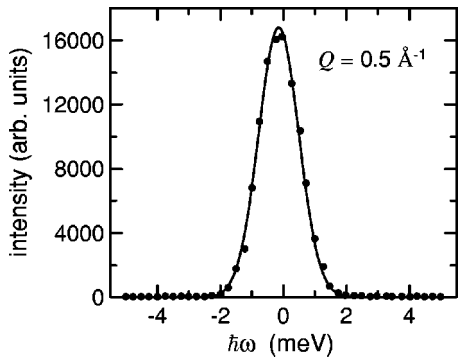

FIG. 4. Raw intensity of the vanadium standard versus energy transfer measured at $Q=0.5$ Å^{-1} (triangles). The solid line is a Gaussian with 1.5-meV FWHM, describing the instrument resolution function calculated according to Ref. 29.

$=0.5$ Å^{-1}. To carry out this comparison, the resolution data were normalized to the peak intensity of the potassium sample and Fig. 5 clearly shows that the inelastic regions of the sample were not affected by the highly symmetric and energy-confined resolution function. As a final comment, we observe that the elastic energy resolution of the three-axis spectrometer, as measured by inelastic scans on vanadium, does not depend on the wave-vector transfer Q. Although expected, this property was, nonetheless, checked in the experiment reported in Ref. 30, which was of the same class as the present one, and where inelastic scans on vanadium were collected at different values of Q.

The measured data were treated following the procedure described in Ref. 31, properly adapted to deal with the inelastic case, and applied in previous experiments[16,18,20,30] of the same class as this one. The initial steps were normalization to the monitor counts and subtraction of the background intensity properly multiplied by the sample transmission which, for the present neutron beam ($k_f=4.8$ Å^{-1}), was equal to 0.91. The background free intensity was then corrected for multiple-scattering (MS) effects which, because of the rather low scattering power of the potassium sample ($\sim$10% of the incident neutrons got scattered), were expected to give a small contribution to the measured signal. In

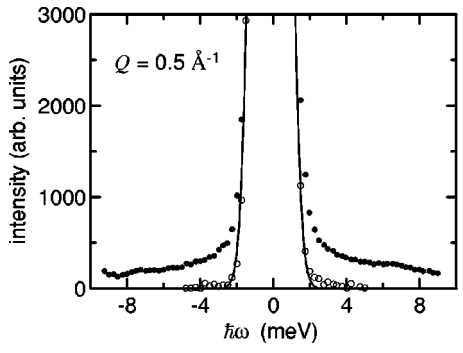

FIG. 5. The vanadium data (circles) and the fitting Gaussian resolution function (solid line) are compared with the raw intensity data of the molten potassium (dots) at $Q=0.5$ Å^{-1} to show the effect expected from the instrument resolution on the side structures of the inelastic spectrum.

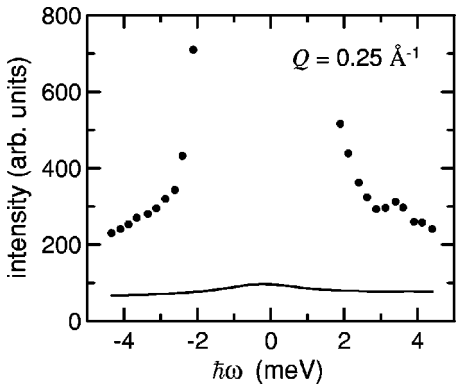

FIG. 6. Background corrected intensity of molten potassium (dots) compared with the calculated multiple-scattering contribution (solid line) at $Q=0.25$ Å^{-1}.

principle, the correction for MS requires the knowledge of the dynamic structure factor $S(Q,\omega)$ of the sample for virtually every Q and ω values. Since these data are not available, except over limited (Q,ω) regions, and in view of the low MS expected in potassium, the response function $S(Q,\omega)$ was modeled and used as input of a simulation program for an iterative MS correction. Prior to the choice of the trial $S(Q,\omega)$ was the assumption that, at the high wave vectors which could also be involved in multiple-scattering processes, the incoherent approximation[13] gives an adequate description of the inelastic cross section. As input of the initial simulation cycle, we selected the dynamic structure factor discussed by Lovesey,[13] which was found to give a satisfactory fit of the incoherent contribution in the case of molten lithium,[3] that is,

$$S_{mod}^{MS}(Q,\omega)=S_{inc}(Q,\omega)$$
$$=\frac{1}{\pi}\frac{\omega\beta}{1-\exp(-\hbar\omega\beta)}$$
$$\times\frac{\tau\delta_1\delta_2}{[\omega\tau(\omega^2-\delta_1-\delta_2)]^2+(\omega^2-\delta_1)^2}, \quad (1)$$

where $\beta=(k_BT)^{-1}$, $\delta_1=Q^2(M\beta)^{-1}$, $\delta_2=2Q^2(M\beta)^{-1}+\Omega^2(0)$, and $\tau^{-1}=\xi\sqrt{\delta_2}$. The quantities $\Omega^2(0)$ and ξ are determined by taking the fourth moment of $S_{inc}(Q,\omega)$ and the $\omega=0$ result for $S_{inc}(Q,\omega=0)$, respectively. Making use of the above model function, the MS contribution was calculated, convoluted with the instrument resolution function and subtracted from the background free data. The resulting difference could be used as input of the next MS calculation cycle, however, in this case, the MS contribution was very low and it was not necessary to iterate the procedure. As an example, the calculated MS contribution is shown in Fig. 6 against the experimental data at $Q=0.25$ Å^{-1}. The order of magnitude of the calculated MS contribution was $\sim$3.5% of the total scattering contribution at that Q value and no wave-vector dependence was found over the Q region of the present experiment. This result can be qualitatively understood by recognizing that, although the number of neutrons that suffer more than one scattering process can be high,

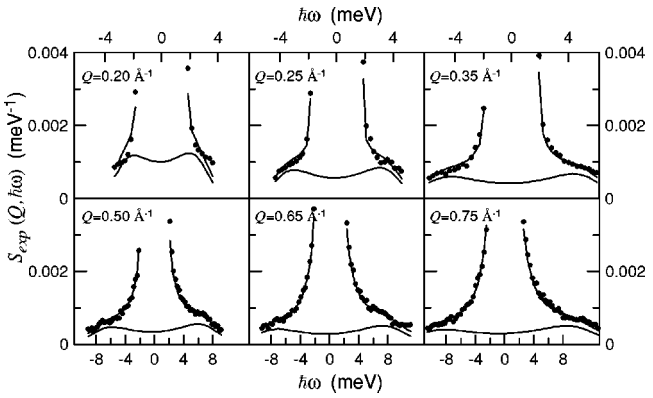

FIG. 7. Dynamic structure factor $S_{exp}(Q,\hbar\omega)$ of molten potassium versus energy transfer and at the lowest measured wave vectors. The experimental data (dots) and the best-fitting curves (lines), calculated according to the phenomenologic model described in the text, are shown on an expanded scale. The DHO contribution (see text) is also shown in each panel.

these processes occur at high wave vectors and, hence, large-energy transfers. Therefore, the contribution of the MS scattered neutrons, which have a high-energy distribution, turns out to be low over the rather low and confined energy window of the present constant-Q experimental scans.

To obtain the dynamic structure factor, the data, corrected for MS and sample transmission, were normalized by exploiting the equivalence of the energy integral of $S(Q,\omega)$ to $[\sigma^{inc}/\sigma^{sc}+(4\pi b^2)S(Q)/\sigma^{sc}]$ with σ^{inc}, σ^{sc}, b, and $S(Q)$, the incoherent and the total scattering cross sections, the coherent scattering length, and the static structure factor of potassium, respectively. The experimental data of $S(Q)$, measured in Ref. 23, were used for the normalization integral. As a check of this procedure, the normalization to vanadium was also applied and, within the error bars of the experiment, the same absolute scale data were obtained. The experimental dynamic structure factor $S_{exp}(Q,\hbar\omega)$ of potassium, put on absolute scale, is shown in Figs. 7 and 8 versus energy transfer and at the wave-vector transfers Q of the measurements. The main features of the experimental $S_{exp}(Q,\hbar\omega)$, which is the cross section weighted sum of the dynamic structure factor and its self part, are a rather sharp quasi elastic peak and inelastic structures aside of this. The inelastic components are related to the collective dynamics of the system and are more pronounced at small-Q values. The quasielastic contribution becomes predominant at large wave-vector transfers, with broad tails which cannot be described by a simple Lorentzian function modeling the quasielastic signal centered at zero energy. At this stage of the data reduction, the complex structure of the quasi elastic signal was apparent from the wave-vector evolution of the experimental $S_{exp}(Q,\hbar\omega)$ spectra. A thorough investigation of the quasielastic spectrum in molten potassium is reported in Ref. 2, where the very high-energy resolution of the measurements ($\sim 10^{-2}$ meV and ~ 0.4 meV) enabled an accurate recognition of two sharp contributions to the quasielastic structure. The present 1.5-meV resolution, largely exceeding the Ref. 2 values, was, on the other hand, optimized to study the propagation of the collective mode in molten potassium.

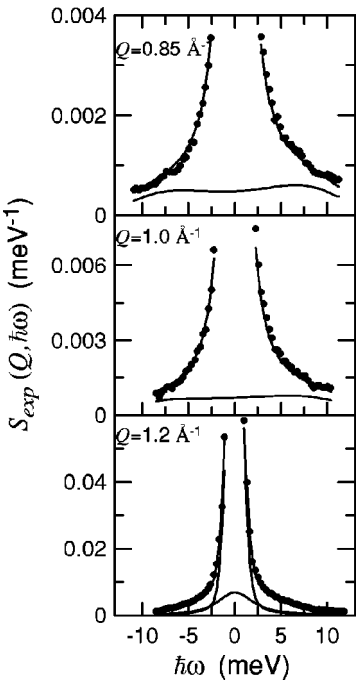

FIG. 8. Dynamic structure factor $S_{exp}(Q,\hbar\omega)$ of molten potassium versus energy transfer and at the largest measured wave vectors. The experimental data (dots) and the best-fitting curves (lines), calculated according to the phenomenologic model described in the text, are shown on an expanded scale. The DHO contribution (see text) is plotted at $Q=0.85$ and 1.0 Å^{-1}. The solid lines shown at the highest-Q value, namely, 1.2 Å^{-1}, are the Lorentzian functions best fitting the quasielastic contribution (see text).

The analysis of the present data could proceed along the formal approach based on the memory-function description of the atomic correlations, which is related to the dynamic structure factor by the following relationship[13]

$$S_{inc/coh}(Q,\omega)=\frac{1}{\pi}S_{inc/coh}(Q)\,\frac{\hbar\omega/k_BT}{1-\exp(-\hbar\omega/k_BT)}\times \mathrm{Re}\left\{\frac{1}{i\omega+\tilde{M}_{i/c}(Q,i\omega)}\right\},$$

where Re indicates the real part of the following expression and $\tilde{M}_{i/c}(Q,s)$ is the Laplace transform of the memory function $M_{i/c}(Q,t)$ defined in the time domain. Use of this equation, which is formally exact, involves the knowledge of the memory function for which no general form is available, although an appropriate equation of motion can be written. Therefore, the practical use of this equation requires an approximation of the memory function by different expressions, which typically provide a rational form for the energy-symmetrized dynamic structure factor.[2,13,14] The expression given in Eq. (1), used to model the dynamic structure factor for the MS correction, is an example of a memory-function approach; indeed, it can be obtained by truncating the continued fraction describing $M_i(Q,t)$ at the second level.[13] In view of the fact that such a formal approach is reduced to approximations of practical use by an empirical modeling of the memory function,[8,9] and considering that use of a rational function for the dynamic structure factor necessarily leads to

the inclusion of only a finite number of frequency moments, we preferred to use an empirical fitting of the measured $S_{exp}(Q,\hbar\omega)$, which describes the essential of the complex liquid dynamics in a simple phenomenologic way.

Therefore, we modeled the dynamic structure factor by means of a damped harmonic oscillator (DHO) to describe the inelastic coherent component of the response related to the collective ion density fluctuations and by Lorentzian functions to account for the quasielastic scattering due to both coherent and incoherent cross sections. The model function $S_{mod}(Q,\omega)$ was convoluted with the four-dimensional $(\mathbf{Q},\omega)$-dependent resolution function of the spectrometer and then fitted to the experimental data. As a first attempt, $S_{mod}(Q,\omega)$ was obtained as a superposition of a DHO and a single Lorentzian function with a FWHM either equal to $2DQ^2$, where D is the self-diffusion constant, or left as one of the free parameters of the fit. This initial choice could appear rather naive, especially in view of the recognized double contribution, coherent and incoherent, to the quasielastic structure, which is discussed in Ref. 2. However, the analysis of Ref. 2 showed that both these components were well described by the two sharp Lorentzian functions with linewidths of comparable size and smaller than ~ 0.65 meV for wave vectors Q ranging from 0 to 1.2 Å^{-1}, that is much smaller than the present instrument resolution (1.5 meV). Therefore, because of the broad energy resolution, a single sharp Lorentzian function was reasonably expected to account for both the two sharp components of the quasielastic peak. We also observe that this was a minimal choice for the fitting procedure which, if adequate to describe the experimental data, would result into a simple computational scheme retaining, however, the physics of the sample as it appears under the present experimental conditions. The results of this fitting scheme were not satisfactory because of the failure in providing good quality fits of the data at every measured wave vector. The next step consisted of adding a second Lorentzian function to account for the additional intensity appearing as extended wings of the quasielastic peak. This option resulted in a satisfactory fit of all the data, with the two Lorentzians accounting for the observed narrow and broad features of the quasielastic spectrum. We remark that the second Lorentzian was modeling a contribution much broader than the quasielastic peaks discussed in Ref. 2, and even broader than the entire energy range of the scan shown in Ref. 2 (inset in Fig. 1 of Ref. 2). The fitting procedure was still simple, with a limited number of free parameters.

The final model for fitting the experimental data was then

$$S_{mod}(Q,\omega)=\left[\frac{\beta\hbar\omega}{1-\exp(-\beta\hbar\omega)}\right]\left[\frac{a_0(Q)}{\pi}\,\frac{\Gamma_0(Q)}{\omega^2+\Gamma_0^2(Q)}+\frac{a_1(Q)}{\pi}\,\frac{\Gamma_1(Q)}{\omega^2+\Gamma_1^2(Q)}\right]+[n(\omega)+1]\frac{a_c(Q)\Gamma_c(Q)\omega}{[\omega^2-\omega_c^2(Q)]^2+\Gamma_c^2(Q)\omega^2} \tag{2}$$

where $n(\omega)$ is the Bose factor, and the collective mode is characterized through the amplitude $a_c(Q)$, the damping parameter $\Gamma_c(Q)$, and the associated energy $\hbar\omega_c(Q)$. $a_0(Q)$ and $a_1(Q)$ are the amplitudes of the two Lorentzian quasielastic peaks having widths $\Gamma_0(Q)$ and $\Gamma_1(Q)$. In the long-wavelength limit, the quasielastic incoherent peak must reduce to a single Lorentzian with FWHM equal to $2DQ^2$, which amounts to $a_1(Q)$ becoming negligible and $\Gamma_0(Q)$ equalling DQ^2. However, considering that the diffusion constant of potassium[32] at 350K is equal to 5.14×10^{-5} cm^{2}s^{-1}, $2DQ^2$ was not negligible with respect to the present resolution. Hence, a more suitable approximation for $\Gamma_0(Q)$, to be used in the fitting procedure, is

$$\Gamma_0(Q)=\frac{DQ^2}{1+\tau_0 DQ^2},$$

where τ_0 has the role of a residence time in the jump-diffusion approximation.

The fitting procedure was carried out in two steps. First of all, the experimental data were fitted to Eq. (2) at each wave-vector value, leaving $a_0(Q)$, $a_1(Q)$, τ_0, $\Gamma_1(Q)$, $a_c(Q)$, $\omega_c(Q)$, and $\Gamma_c(Q)$ as free parameters. It was found that $a_1(Q)$ decreases with decreasing Q, while $\Gamma_1(Q)$ does not sensibly depend on Q. This result was already observed in liquid mercury,[18] where the same trend for the broad quasielastic peak was found, although the intensity of the broad component was much higher in that case. The second step of the fitting procedure consisted of holding $\Gamma_1(Q)$ fixed, in order to reduce the number of free parameters. With this option, good fits were obtained at every Q's except the largest one ($Q=1.2$ Å^{-1}), where an unsatisfactory amplitude for the DHO contribution was obtained mostly because of the too limited experimental energy range. The curves calculated using the best-fit parameters are also shown in Figs. 7 and 8 together with the experimental data. This comparison shows that the quality of the fits is very good, apart from the mentioned limits at $Q=1.2$ Å^{-1}. We repeat that this method, although of empiric nature like other models often used to describe the dynamic structure factor, is the simplest one containing all the qualitative features observed in the experimental data.

A close inspection of the fits reveals that the results are compatible with the presence of a collective mode in the experimental data for wave vectors up to $Q=1$ Å^{-1}. The dispersion of the collective modes, as defined by the Q dependence of the fitting parameter $\hbar\omega_c(Q)$, is shown in Fig. 9. We note that this interpretation is well founded on the DHO model.[33] Moreover, we preferred this phenomenologic way of deducing the dispersion relation of the density fluctuations to the one based on the maxima of the longitudinal current correlation function $J_L(Q,\omega)=(\omega^2/Q^2)S(Q,\omega)$, because $J_L(Q,\omega)$ must have a peak the position of which is not necessarily related to collective mode, and it can be affected by possible systematic errors present on the wings of $S(Q,\omega)$. In order to determine the velocity of the collective excitations, we applied a linear fit to the dispersion in the low-Q region. The velocity turned out to be 15.5 ±0.5 meV/Å^{-1}, that is, 2360 ± 80 m/s. This value is 30%

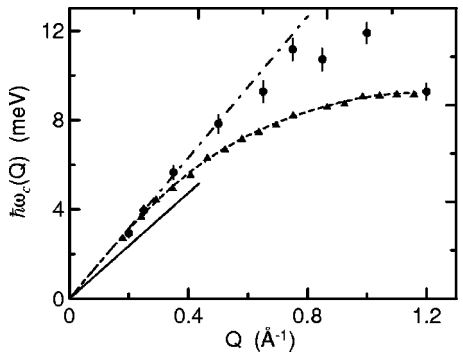

FIG. 9. Dispersion relation $\hbar\omega_c(Q)$ associated with the collective vibration as obtained from the present model (dots), linear dispersion relation associated with the sound velocity $v_{sound}=11.85$ meV Å (solid line), and phonon-dispersion curve along the [100] direction in crystalline potassium at 9 K (triangles). The dashed line joining the triangles is obtained by a force-constant fit to the experimental phonon data, and the phonon velocity, resulting from the linear extrapolation of this curve to low Q, is 16.2 meV Å. The dot-dashed line is the best fit to the low-Q portion of the dispersion curve in molten potassium, which provided a collective-mode velocity $v_{coll}=15.5$ meV Å.

higher than the isothermal sound velocity[22] at the same temperature, which is 1800 m/s. Such a result is not new in alkali metals, where a velocity of collective modes exceeding the sound velocity was reported in all cases. In Fig. 9, the phonon-dispersion curve as measured in solid crystalline potassium[24] along the [100] direction at 9 K is also shown. The substantial agreement between the present data in the liquid phase and the phonon-dispersion curve in solid potassium suggests that the high-frequency component of the dynamic structure factor of the liquid has some solidlike character, although the collective mode is strongly damped in the liquid. Moreover, we observe that the density of potassium at 9 K does not differ considerably from that of the liquid at 350 K, namely, 0.92 g cm^{-3} against 0.82 g cm^{-3}, with the consequence of average interatomic distances and interatomic forces being rather similar in the two phases.

It is also interesting to analyze the strength of the collective mode as obtained from the integral

$$Z_c(Q)=\int_{-\infty}^{+\infty} d\omega \frac{a_c(Q)\Gamma_c(Q)\omega}{[\omega^2-\omega_c^2(Q)]^2+\Gamma_c^2(Q)\omega^2}[n(\omega)+1].$$

This integral is particularly meaningful in the wave-vector region $0.25\leqslant Q\leqslant 1$ Å^{-1}, where a sufficiently wide energy range was covered in the experiment and the DHO contribution was unambiguously obtained from the fitting procedure. The ratio of $Z_c(Q)$ to the static structure factor $S(Q)$ is shown in Fig. 10, where a rather constant trend versus Q can be observed over the whole Q range. In general, $Z_c(Q)$ accounts for about 25% of the static structure factor.

The strength associated with the quasielastic contribution was obtained by calculating the integrated intensities under the two Lorentzian functions used in the fit, that is

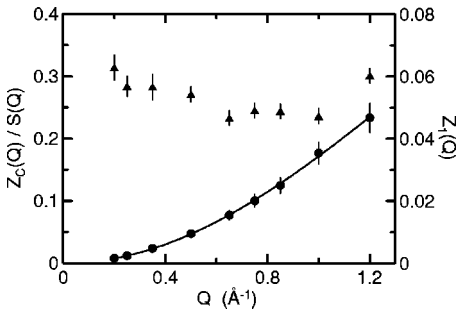

FIG. 10. Wave-vector dependence of the ratio between the strength of the collective-mode contribution $Z_C(Q)$ and the static structure factor $S(Q)$: triangles and y axis on the left. Wave-vector dependence of the strength $Z_1(Q)$ of the broad Lorentzian component of the present fit: dots and y axis on the right. The continuous line is the model function $f=f_0[1-\sin(Qd)/(Qd)]$ fitting the $Z_1(Q)$ data (see text).

$$Z_{0/1}(Q)=\int_{-\infty}^{+\infty} d\omega \frac{\beta\hbar\omega}{1-\exp(-\beta\hbar\omega)} \frac{a_{0/1}(Q)}{\pi} \frac{\Gamma_{0/1}(Q)}{\omega^2+\Gamma_{0/1}^2(Q)}.$$

As to the sharp Lorentzian function, an almost Q-independent strength $Z_0(Q)\sim 0.2$ was found, although we note that the experimental energy resolution was too broad to get an accurate evaluation of the width $\Gamma_0(Q)$. From the fit a residence time $\tau_0=2.0\pm 0.7$ ps was obtained, however, this value depends on the chosen expression for $\Gamma_0(Q)$. Despite the limited accuracy of the present estimate of $\Gamma_0(Q)$, in Fig. 11 we compare our results with those measured in Refs. 2 and 5, which were obtained at higher resolution. An overall good agreement between the three sets of experimental data can be observed over the Q range presently explored, although the data of Ref. 2 should be taken as the reference for the incoherent quasielastic linewidths. The observed agreement with the incoherent scattering results of Ref. 2 suggests that our quasielastic sharp contribution to the dynamic structure factor was dominated by the incoherent scattering term. As regards the broad Lorentzian function, which was neces-

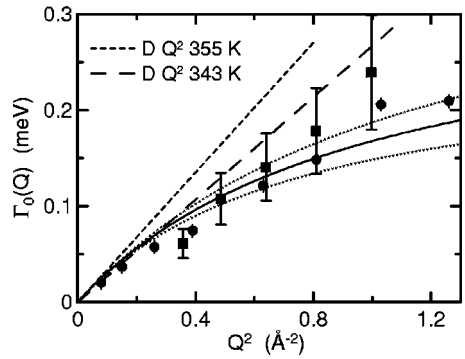

FIG. 11. Width $\Gamma_0(Q)$ of the sharp Lorentzian component of the present fit to the potassium data (solid line), calculated using the best-fit value of τ_0 (see text). The two dotted lines enclosing the curve of $\Gamma_0(Q)$ represent an estimate of the maximum error region. The higher-resolution data from Refs. 2 (squares) and 5 (dots) are also shown. The two dashed lines are the long-wavelength diffusion limits of the width, at two temperature values.

TABLE I. Sound velocity v_{sound} RPA prescription for the collective-mode velocity v_{RPA} and *experimental* collective-mode velocity v_{coll} deduced from the present common analysis of neutron and x-ray data on molten alkali metals (see text). r_s is the parameter related to the electron density and defined in the text.

	r_s	v_{sound} (meV Å)	v_{RPA} (meV Å)	v_{coll} (meV Å)	v_{coll}/v_{sound}	v_{coll}/v_{RPA}
Li	3.303	28.77	42.80	36.5±1.8	1.27±0.06	0.85±0.04
Na	4.053	15.81	19.16	18.5±1.5	1.17±0.09	0.97±0.08
K	5.021	11.85	11.86	15.5±0.8	1.31±0.07	1.31±0.07
Rb	5.355	7.87	7.52	9.2±0.5	1.17±0.06	1.22±0.07
Cs	5.776	6.02	5.59	7.5±0.6	1.25±0.10	1.34±0.10
$Li(ND_3)_4$	7.400	9.40	5.39	11.2±0.2	1.19±0.02	2.08±0.04

sary to describe the rather extended quasielastic wings of the experimental data, the analysis of the strength showed that the integrated intensity $Z_1(Q)$ represented a very small contribution to the overall quasielastic structure, although it was characterized by a remarkable Q dependence. The results obtained for $Z_1(Q)$ are shown in Fig. 10 (y axis on the right), where it is apparent that $Z_1(Q)$ is an increasing function of the wave-vector transfer. The ratio of $Z_1(Q)$ to the almost Q-independent $Z_0(Q)$ goes from some negligible 1–2% at low-Q values, to ~20% at the highest-Q values of the experiment. Moreover, we remind that a result of the fit was the width $\Gamma_1(Q)$ of the broad Lorentzian being scarcely dependent on Q. Indeed, the FWHM was taken as independent of Q and held constant in the fit, namely, $2\Gamma_1(Q) = 2\Gamma_1 = 4.0 \pm 0.4$ meV. These characteristics, that is, the Q-dependent integrated intensity and the Q-independent linewidth, prevent any easy association of the broad component with a free diffusion in real space. On the other hand, the FWHM equal to ~4 meV, which largely exceeds the linewidth of the coherent quasi elastic Q-dependent component investigated in Ref. 2, namely, ~0.5 meV average value over the Q range 0–1.2 $Å^{-1}$, keeps from identifying the broad quasielastic component with the purely coherent heat mode.

The interpretation of the quasielastic structures observed in the present measurements, which, we remark once more, was not the aim of the experiment, is not straightforward because of the broad energy resolution. Referring to the results of Ref. 2 on the quasielastic linewidths, we believe that the coherent and incoherent quasielastic components, discussed, both make their contribution into our sharp Lorentzian peak and, because of our experimental configuration, they cannot be disentangled from one another. From the comparison of the $\Gamma_0(Q)$ data shown in Fig. 11, and observing that the ratio $\sigma^{coh}S(Q)/\sigma^{inc}$ is smaller than ~0.2 for Q ranging from 0 to 0.5 $Å^{-1}$, we can conclude that the incoherent contribution is governing our sharp Lorentzian peak. Finally, recalling that the collective-mode strength Z_c amounts to about 25% of $S(Q)$, we expect that a large fraction of the broad Lorentzian term is brought about by coherent quasielastic processes. All these observations suggest for the quasielastic scattering a rather complex underlying structure, which certainly deserves further experimental investigation. We simply observe that a plausible picture, consistent with the observed features of the broad Lorentzian contribution, could be that of some fast time-scale dynamics with an associated characteristic time equal to $1/\Gamma_1 = 0.32 \pm 0.03$ ps. Since the relation of this dynamic process to a free-diffusion in real space is ruled out by the Q dependencies of $Z_1(Q)$ and $\Gamma_1(Q)$, one could interpret it as a fast motion taking place over a confined region. Following this conjecture, we described the motion confined over a distance d by means of the simple model function $f = f_0[1 - \sin(Qd)/(Qd)]$, with f_0 and d parameters of the fit to the experimental $Z_1(Q)$ data. We found $d = 2.0 \pm 0.5$ Å. The resulting curve is also shown in Fig. 10 in comparison with the $Z_1(Q)$ data.

III. CONCLUSION AND FINAL REMARKS

Since the present study aims at establishing the relationship between the collective vibration at THz frequencies of the ions in the liquid metal and the electron screening effects, we focused the analysis on the velocity associated with the collective mode. As reported in the preceding section, the velocity is about 30% higher than the sound velocity and this anomaly is similar to what was observed in the other alkali metals. To obtain some model-independent conclusions and unambiguous features common to the dynamics of all the alkali metals near the melting point, we applied the present fitting procedure to the experimental data available from literature, obtained by inelastic neutron[1,6,7,20] and by inelastic x-ray scattering[8,9] in molten alkali metals. This procedure ensures the accessibility to a unique and internally consistent set of mode velocity data, obtained by a linear fit of the low-Q dispersion curves, which, in turn, were obtained by plotting the DHO best-fit vibration energies $\hbar\omega_c(Q)$. The velocities associated with the collective mode observed in the five alkali metals, and resulting from the present analysis, are summarized in Table I in comparison with the sound velocity at the melting point and the values of the velocities calculated in the framework of the RPA using the BS approximation,[17,21] that is

$$v_{RPA} = \lim_{Q \to 0} \sqrt{\frac{\Omega_p^2}{\epsilon(Q)Q^2}}$$

where Ω_p is the ion plasma frequency and $\epsilon(Q)$ is the static RPA dielectric function of the electron gas. In Table I the ratios of the *experimentally* determined velocity of the collective modes to that calculated and to the sound velocity are

also reported. While the latter ratio is, as expected, always larger than one and no simple systematic trend with the electron density or the atomic number can be safely identified, the former ratio is less than one for the light metals, while it is close to 1.3 for K, Rb, and Cs. The data of Table I show that a quantitative description of the velocity of the collective modes cannot be obtained within the simplified BS model. It is interesting to comment on the accurate account of the velocity value given by RPA in the case of Na. Although Na has been considered for long as the prototype of an almost free-electron metal, we think that the observed agreement is rather accidental, since RPA is expected to fail at the already too low density of Na (namely $r_s=4.05$, with $r_s a_0 = (3/4\pi n)^{1/3}$, n is the electron number density and a_0 is the Bohr radius) which causes the electron-electron interaction to dominate over the kinetic energy of the interacting electron gas.

The inadequacy of a RPA approach to treat the electron correlations was strikingly evident in the case of a saturated metallic solution of lithium in deuterated ammonia, which is a very low-density liquid metal ($r_s=7.4$). The experimental results in lithium ammonia could be interpreted by a more sophisticated treatment of the electron-electron interactions, namely, an approximation to the dielectric function beyond the RPA including local-field corrections.[21] We remind that the BS model was found to work quite accurately in the case of liquid mercury and lead, that is, two high-electron-density systems ($r_s^{Hg}=2.70, r_s^{Pb}=2.97$). We believe that the agreement for Na could be due to an accidental cancellation of two terms, one stemming from the electrons and corrective to the RPA, and the other from the ion potential.

The observed overall behavior can be considered as a strong indication that a more accurate theoretical modeling is necessary for a full account of the experimental findings in the THz frequency regime. An improved treatment of the electron gas and the screening effects on the ion-ion interactions is necessary, and probably sufficient, since it will introduce important differences between high and low electron-density systems, that is, regimes of low and high coupling.

In conclusion, we investigated the collective dynamics of liquid potassium in the region of low wave-vector transfers by means of inelastic neutron scattering. The experiment confirmed the anomalous dispersion of the collective modes, resembling that observed in other alkali metals. A comparative analysis of all molten alkali metals, carried out by applying the same fitting procedure to the experimental data from Refs. 1,6–9, and 20, showed that an improved treatment of the dielectric screening is necessary to account for the low-Q low-frequency dynamics of the low electron-density alkali metals. Moreover, we observe that the dispersions shown in Fig. 9 seem to suggest a reduction of the collective-mode velocity at the lowest wave-vector transfer studied in the present investigation, namely, $Q=0.2$ Å^{-1}. Indeed, $Q=0.2$ Å^{-1} seems to be the edge of the transition region from the hydrodynamic to the higher-frequency regime. However, this point deserves further experimental investigation at even lower-Q values.

As a final remark, we observe that potassium is a good candidate for a complementary neutron and x-ray inelastic scattering investigation. Indeed, the different coupling of the two probes to atomic nuclei and electron cloud, respectively, leading to information on the nuclear dynamics, could be investigated in this liquid metal, which is easily accessible to both experimental techniques. Moreover, exploiting the intrinsically coherent nature of the x-ray experiments, a more extended analysis of the coherent and incoherent contributions could result from the comparison with the neutron experiments.

[1] J.R.D. Copley and J.M. Rowe, Phys. Rev. Lett. **32**, 49 (1974); Phys. Rev. A **9**, 1656 (1974).

[2] C. Cabrillo, F.J. Bermejo, M. Alvarez, P. Verkerk, A. Maira-Vidal, S.M. Bennington, and D. Martin, Phys. Rev. Lett. **89**, 075508 (2002).

[3] P. Verkerk, P.H.K. de Jong, M. Arai, S.M. Bennington, W.S. Howells, and A.D. Taylor, Physica B **180-181**, 834 (1992); P.H.K. de Jong, P. Verkerk, and L.A. de Graaf, J. Phys.: Condens. Matter **6**, 8391 (1994); J. Non-Cryst. Solids **156**, 48 (1993).

[4] C. Morkel and W. Glaser, Phys. Rev. A **33**, 3383 (1986); C. Morkel, C. Gronemeyer, W. Glaser, and J. Bosse, Phys. Rev. Lett. **58**, 1873 (1987); U. Balucani, A. Torcini, A. Stangl, and C. Morkel, J. Non-Cryst. Solids **205-207**, 299 (1996); A. Stangl, C. Morkel, U. Balucani, and A. Torcini, *ibid.* **205-207**, 402 (1996).

[5] A.G. Novikov, V.V. Savostin, A.L. Shimkevich, R.M. Yulmetyev, and T.R. Yulmetyev, Physica B **228**, 312 (1996); A.G. Novikov, V.V. Savostin, A.L. Shimkevich, and M.V. Zaezjev, *ibid.* **234-236**, 359 (1997); A.G. Novikov, M.N. Ivanovskii, V.V. Savostin, A.L. Shimkevich, O.V. Sobolev, and M.V. Zaezjev, J. Phys.: Condens. Matter **8**, 3525 (1996).

[6] P. Chieux, J. Dupuy Philon, J.F. Jal, and J.-B. Suck, J. Non-Cryst. Solids **205-207**, 370 (1996); G. Pratesi, J.-B. Suck, and P.A. Egelstaff, *ibid.* **250-252**, 91 (1999).

[7] C. Morkel and T. Bodensteiner, J. Phys.: Condens. Matter **2**, 251 (1990); T. Bodensteiner, Chr. Morkel, W. Gläser, and B. Dorner, Phys. Rev. A **45**, 5709 (1992).

[8] H. Sinn, F. Sette, U. Bergmann, Ch. Halcoussis, M. Krisch, R. Verbeni, and E. Burkel, Phys. Rev. Lett. **78**, 1715 (1997); T. Scopigno, U. Balucani, G. Ruocco, and F. Sette, J. Phys.: Condens. Matter **12**, 8009 (2000); Phys. Rev. Lett. **85**, 4076 (2000).

[9] W.-C. Pilgrim, S. Hosokawa, H. Saggau, H. Sinn, and E. Burkel, J. Non-Cryst. Solids **250-252**, 96 (1999); T. Scopigno, U. Balucani, G. Ruocco, and F. Sette, Phys. Rev. E **65**, 031205 (2002).

[10] L. Sjögren and A. Sjölander, J. Phys. C **12**, 4369 (1979); L. Sjögren, *ibid.* **13**, 705 (1980); G. Wahnström and L. Sjögren, *ibid.* **15**, 401 (1982); L. Sjögren, Phys. Rev. A **22**, 2866 (1980); **22**, 2883 (1980).

[11] K. Kawasaki, Ann. Phys. (N.Y.) **61**, 1 (1970); T. Keyes, in *Statistical mechanics*, edited by B.J. Berne (Plenum Press, New York, 1977), part B.

[12] H. Mori, Prog. Theor. Phys. **33**, 423 (1965); **34**, 399 (1965).

[13] S.W. Lovesey, *Theory of Neutron Scattering from Condensed*

Matter (Oxford University Press, Oxford, 1986), Vol. 1.
[14] U. Balucani and M. Zoppi, *Dynamics of the Liquid State* (Clarendon Press, Oxford, 1994).
[15] N.H. March, *Liquid Metals* (Cambridge University Press, Cambridge, 1990).
[16] L.E. Bove, F. Sacchetti, C. Petrillo, and B. Dorner, Phys. Rev. Lett. **85**, 5352 (2000).
[17] D. Pines and Ph. Nozieres, *The Theory of Quantum Liquids* (Benjamin, New York, 1966).
[18] L.E. Bove, F. Sacchetti, C. Petrillo, B. Dorner, F. Formisano, and F. Barocchi, Phys. Rev. Lett. **87**, 215504 (2001).
[19] C.A. Burns, P.M. Platzman, H. Sinn, A. Alatas, and E.E. Alp, Phys. Rev. Lett. **86**, 2357 (2001).
[20] F. Sacchetti, E. Guarini, C. Petrillo, L.E. Bove, B. Dorner, F. Demmel, and F. Barocchi, Phys. Rev. B **67**, 014207 (2003).
[21] G.D. Mahan, *Many-Particle Physics* (Plenum, New York, 1991).
[22] *Handbook of Thermodynamic and Transport Properties of Alkali Metals*, edited by R.W. Ohse (Academic, Oxford, 1985).
[23] A.J. Greenfield, J. Wellendorf, and N. Wiser, Phys. Rev. A **4**, 1607 (1971); M.J. Huijben and W. van der Lugt, Acta Crystallogr., Sect. A: Cryst. Phys., Diffr., Theor. Gen. Crystallogr. **35**, 431 (1979).
[24] R.A. Cowley, A.D.B. Woods, and G. Dolling, Phys. Rev. **150**, 487 (1966); W.J.L. Buyers and R.A. Cowley, *ibid.* **180**, 755 (1969).
[25] S.K. Lai, Wang Li, and M.P. Tosi, Phys. Rev. A **42**, 7289 (1990).
[26] H.R. Glyde, J.P. Hansen, and M.L. Klein, Phys. Rev. B **16**, 3476 (1977).
[27] Ki-dong Oh and P.A. Deymier, Phys. Rev. Lett. **81**, 3104 (1998); Phys. Rev. B **59**, 11 276 (1999).
[28] M. Hansen, *Constitution of Binary Alloys*, 2nd ed. (McGraw-Hill, New York, 1958), p. 102.
[29] M.J. Cooper and R. Nathans, Acta Crystallogr. **23**, 357 (1967); B. Dorner, Acta Crystallogr., Sect. A: Cryst. Phys., Diffr., Theor. Gen. Crystallogr. **28**, 319 (1972).
[30] C. Petrillo, F. Sacchetti, B. Dorner, and J.-B. Suck, Phys. Rev. E **62**, 3611 (1999).
[31] C. Petrillo and F. Sacchetti, Acta Crystallogr., Sect. A: Found. Crystallogr. **46**, 440 (1990).
[32] *Handbook of Chemistry and Physics*, 79th ed. (CRC Press, Boca Raton, FL, 2000).
[33] B. Fåk and B. Dorner, Institut Laue-Langevin Internal Report No. ILL92FA08T 1992 (unpublished); B. Fak and B. Dorner, Physica B **234-236**, 1107 (1997).